Monatshefte für Chemie 138, 285–291 (2007)
DOI 10.1007/s00706-007-0619-0
Printed in The Netherlands

Monatshefte für Chemie
Chemical Monthly

Modeling the Kinetics of Hydrosilylation Based Polyaddition

Nicolas C. Imlinger[1,2,3], **Manfred Krell**[1,*], and **Michael R. Buchmeiser**[2,3,*]

[1] Wacker Chemie AG, Burghausen, Germany
[2] Leibniz-Institute of Surface Modification e. V. (IOM), Leipzig, Germany
[3] Institute of Technical Chemistry, University of Leipzig, Leipzig, Germany

Received February 1, 2007; accepted (revised) February 14, 2007; published online March 29, 2007

Summary. Platinum(II) chloride was used in the hydrosilylation of 1,1,3,3-tetramethyldisiloxane and divinylbenzene. The reaction was monitored online by FTIR spectroscopy and reaction kinetics were determined by Self Modeling Curve Resolution (SMCR). The hydrosilylation polymerization follows a second order polyaddition kinetics with $k = 2.03 \times 10^{-4}\ \mathrm{dm^3\,mol^{-1}\ s^{-1}}$.

Keywords. Polymerization; Self modeling curve resolution (SMCR); Factor analysis; IR spectroscopy; Homogenous catalysis.

Introduction

Hydrosilylation is the most important technique to form Si–C bonds and describes the addition of silicon hydrides to double or triple bonds [1]. Already *Speier et al.* [2] described these usually platinum-catalyzed reactions to be highly exothermic and fast, making thermal management of the reaction crucial and thus, kinetic reaction analysis challenging. Hydrosilylation reactions may also be used for the synthesis of polymeric materials (*cf.* Scheme 1) [3]. Quite often oligomers containing the required functionalities are further polymerized and/or crosslinked by hydrosilylation [4]. Siloxane-elastomers, like polydimethylsiloxane, are commonly synthesized in that way, being an easy-to-use, moldable polymerization-system [5]. In case bifunctional molecules, *i.e.* dienes and diynes, are used, hydrosilylation yields alkylsilane or alkenylsilane polymers (*cf.* Scheme 1, Type B) [6].

The determination of reaction kinetics lies right at the heart of physico-chemical analysis, potentially revealing the molecular mechanism and establishing a mathematical model describing the chemistry under study [7]. This mathematical model forms the basis for reactor design and the subsequent engineering processes implied in producing chemicals on an industrial scale [8]. Reaction kinetics are usually determined by fitting concentration profiles to a linearized model. Concentration profiles are best obtained by online spectroscopy. Application of *Lambert-Beer*'s law

$$E_\lambda = c \cdot \alpha_\lambda \cdot l \tag{1}$$

(E_λ is the absorbance at wavelength λ, c the concentration, α_λ the absorption coefficient at wavelength λ, and l the path length of the light through the sample) permits the calculation of concentration from absorbance; α_λ is normalized and combined with l. When analysis is performed at more than one wavelength (like measuring a whole spectrum) and when the concentration profiles of several species are observed at once, Eq. (1) may be expanded to its multivariate form.

$$D = C \cdot A \tag{2}$$

(D is the data matrix, C the matrix of the concentration profiles, and A the matrix of pure component

* Corresponding authors. E-mail: manfred.krell@wacker.com; michael.buchmeiser@iom-leipzig.de

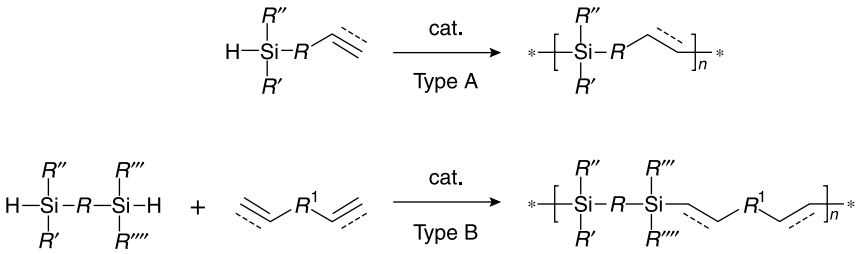

Scheme 1

spectra) D is the common result of online spectroscopic reaction monitoring and has dimension m × n with m being equivalent to time (how often and when spectra have been recorded) and n being the wavenumber (depending on the applied spectroscopy and ranging for our ATR-FTIR-setup from 600–4000 cm^{-1}). Kinetic analysis is only interested in C which is of the dimension m × r with r being the number of reactants (including potential intermediates and by-products) involved. Essentially, using Eq. (1) the reasoning is equivalent; E_λ is measured while the evolution of c with time is of interest for reaction kinetics. The superiority of the multivariate approach is obvious. Equation (1) implies several assumptions (like exact assignment of a single wavelength (peak) to a specific molecule, or peak-purity, etc.) that are cumbersome to ascertain and which simply might not hold. Moreover, an univariate analysis will give the concentration profile of only one component, making a decision on the reaction mechanism and which kinetic model to fit very difficult. For kinetic analysis SMCR is a well suited multivariate approach [9]. SMCR requires bilinear data which essentially corresponds to the form of the data matrix D, composed of multi-wavelength spectra measured at different moments of the time scale [10]. Factor analysis serves as a basis for any SMCR approach [11]; D is reduced to its lowest dimensionality by Principal Component Analysis (PCA, usually calculated by Singular Value Decomposition (SVD)) [12]. This gives a preliminary solution to Eq. (2), which is further refined using SMCR to suffice a sensible chemical context [13].

We report the hydrosilylation polyaddition of 1,1,3,3-tetramethyldisiloxane **1** and divinylbenzene **2**, catalyzed by platinum(II) chloride **3**, and the determination of its reaction kinetics by SMCR. The present system is in analogy to the hydrosilylaton of styrene and triethylsilane using the same platinum source as reported by *Caseri* and *Pregosin* [14]. Our goal is to find out whether the easy-to-use $PtCl_2$-catalyst-system can be employed to yield poly[1,1,3,3-tetramethyl-1-(ethylenephenyleneethylene)disiloxane] **4** and to show the superiority of a multivariate approach for kinetic analysis even when the kinetic model under study is simple and analytically solvable.

Results and Discussion

Figure 1 shows the FTIR-spectra recorded during reaction; this is a projection along the time axis (m-dimension) of D (*cf.* Eq. (2)).

The siliconhydride peak around 2100 cm^{-1} is not suited for quantitative analysis since there is strong background absorbance from the diamond-ATR-crystal in the same region. The fingerprint region shows changing peak intensities with potentially pure peak profiles of a single component. Careful investigation of the educt and solvent spectra suggests that

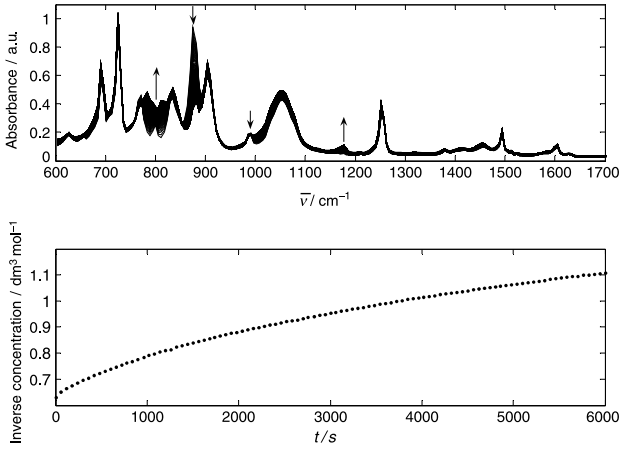

Fig. 1. Fingerprint region of D, projected along the time axis (above). Linearized plot of the peak profile at 878 cm^{-1} (below); it is not possible to reasonably fit a straight line to this peak profile

the peaks at 878 cm^{-1} (assigned to Si–H bending) and at 988 cm^{-1} (assigned to Vinyl-CH_2 wagging) may be suited for univariate analysis (*cf.* Eq. (1)) [15]. IR is not very sensitive to double bonds; therefore the signal at 988 cm^{-1} in Fig. 1 is small and, due to potential overlap with the neighboring siloxane peak, unsuited. From the peak at 878 cm^{-1} a sensible peak profile could be extracted. Assuming a second order kinetic model (typical for polyadditions [16]) a linear dependence of the inverse concentration versus time should be present.

$$\frac{dc}{dt} = k \cdot c^2 \tag{3}$$

This linearized model did *not* fit the peak profile at 878 cm^{-1} (*cf.* Fig. 1) suggesting either a different reaction model or that the signal at 878 cm^{-1} is not a pure component peak. Consequently, we applied SMCR to resolve the reaction kinetics. Several issues need to be addressed in this context [17], which are (i) the potential rank deficiency of D that may arise from collinearity in the concentration profiles; (ii) the determination of principal factors, or in other words the number of reacting species present in D, which implies a suitable kinetic reaction model; and (iii) the question which objective function to use for the optimization algorithm and the identification of sensible starting and boundary values for the optimization algorithm.

Determination of Chemical Rank

D was measured isothermally at 60°C. Rank analysis revealed that D is rank deficient. Mathematically, the rank of a matrix is the number of linearly independent vectors of this matrix [18]; that is, there are linear dependencies in D attributed to the concentration profiles. This is a common problem in chemistry since reactions are seldom monomolecular, but rather have several reagents that react in parallel [19]. *Amrhein et al.* suggested methods for rank augmentation of data matrices [20]. We chose to run a non-isothermal reaction inducing further changes in the concentration profiles. This gave a data matrix $D_{non\text{-}iso}$ for which Eq. (2) is also valid. Different concentration profiles $C_{non\text{-}iso}$ apply but the pure component spectra A remain the same, provided there is no thermal dependency of the spectra. A comparison of the spectra of the reaction mixture at 70°C and at 40°C showed virtually no difference thus, no dependence on temperature. $D_{non\text{-}iso}$ was no longer rank deficient and was analyzed by the Alternating Least Squares algorithm (ALS) [21]. ALS subsequently and iteratively solves the two Eqs. (4) and (5).

$$A_{calc} = C^{+}_{calc} \cdot D_{non\text{-}iso} \tag{4}$$

$$C_{calc} = D_{non\text{-}iso} \cdot A^{+}_{calc} \tag{5}$$

Iteration is stopped when the error matrix F meets the convergence criterion ε, *i.e.* when the difference between the measured matrix $D_{non\text{-}iso}$ and the calculated one D_{calc} (*cf.* Eq. (2)) is minimized.

$$F = D_{non\text{-}iso} - C_{calc} \cdot A_{calc} \tag{6}$$

The results from Abstract Factor Analysis (AFA) [11] were used to start the ALS algorithm. Figure 2 shows the spectra as they were recovered by ALS from $D_{non\text{-}iso}$. Since the pure component spectra must be the same in D and in $D_{non\text{-}iso}$, C can be calculated employing Eq. (5) with A_{calc} and D, and the linearized plot thereof is also shown in Fig. 2.

Principal Factor Analysis

Malinowski was the first to introduce the theory of error to factor analysis [22]. The key task is to separate the true signal from noise (measurement error) using the number of principal factors, which additionally reduces the size of the data matrix to the factor space. Several methods have been developed

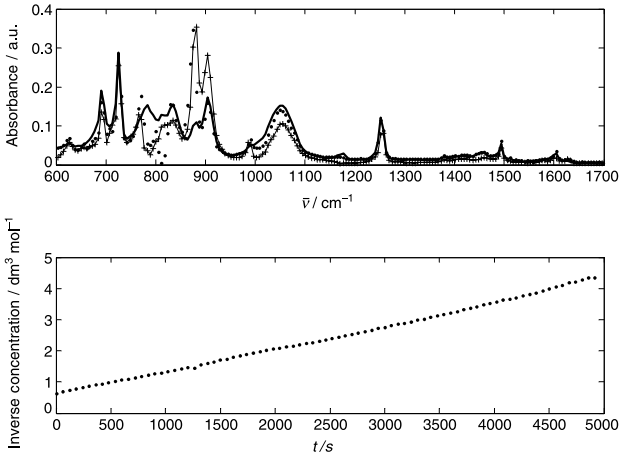

Fig. 2. Fingerprint region of the spectra as recovered by ALS (above). Linearized plot of the concentration profile as recovered by ALS (below); this was subjected to linear regression and k_{init} could be calculated. In the figure above '•' denotes educt **1**, '··+··' denotes educt **2**, and '—' denotes the product

to determine the number of principal factors [11]. *Meloun et al.* compared commonly used methods; the authors determined the Factor Indicator Function (IND) and the index RESO (Ratio of Eigenvalues Calculated by Smoothed PCA and those by Ordinary PCA) to perform best in predicting the number of principal factors [23]. In the present work, additionally to IND and RESO, we applied the Scree test and the plot of eigenvalues (*eig*) from PCA to assess the number of principal factors. In this context we propose a slight modification to the index RESO as published by *Chen et al.* [24].

$$RESO_i = \frac{eig_i^s}{eig_i^o} \tag{7}$$

Instead of Eq. (7) (with eig^s being the eigenvalues of smoothed PCA and eig^o the eigenvalues of ordinary PCA) and plotting the logarithm of RESO, we used the *Durbin-Watson* criterion (*DW*) [25], which shows correlations between consecutive points and becomes higher with increasing randomness.

$$RESO - DW_i = \frac{(eig_i^s - eig_i^o)^2}{eig_i^s \cdot eig_i^o} \tag{8}$$

When comparing eig^s and eig^o pairwise using *DW*, its value will become high as soon as eig^s differs from eig^o. Consequently, a rise to a high value in Eq. (8) indicates the number of principal factors. From our experience, comparing the ratio of eigenvalues calculated by smoothed PCA and those by ordinary PCA using the *Durbin-Watson* criterion, RESO-*DW* (*cf.* Eq. (8)), gives a clearer indication on the number of principal factors.

As can be seen in Fig. 3 the determination of the number of principal factors is less dependent on the smoothing factor, when using RESO-*DW*. The number of principal factors of *D* is clearly assessed to three from RESO-*DW*, whereas there might be some doubt whether the number of principal factors of *D* is two or three when using RESO. The number of principal factors in *D* was calculated using all aforementioned methods and assessed to be three.

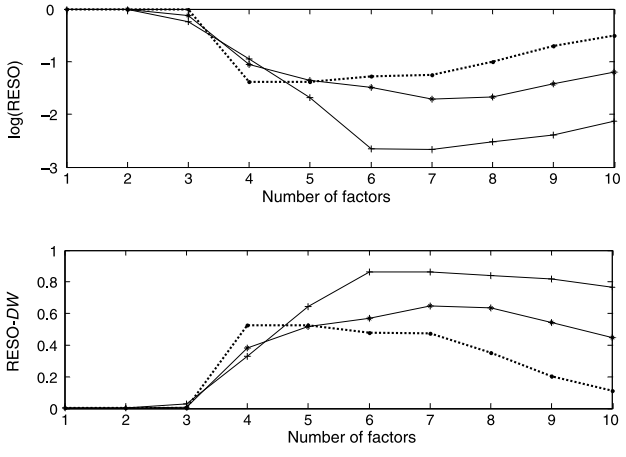

Fig. 3. Plot of the logarithm of RESO (*cf.* Eq. (7)) *versus* the number of factors (above). Plot of RESO-*DW* (*cf.* Eq. (8)) *versus* the number of factors (below). In both cases a deviation from zero level shows the number of principal factors. In both figures the smoothing factors 0.1, 1, and 10 are denoted by '··+··', '··✻··', and '··●··'

Kinetic Optimization and Reaction Analysis

The procedures involved with the ALS algorithm and factor analysis revealed that a second order kinetic model may be safely assumed and gave an initial estimate k_{init} for further optimizations (k_{init} was calculated by linear regression from the gradient of the linearized model shown in Fig. 2). Using k_{init} and a second order kinetic model, concentration profiles C_{target} can be calculated (*cf.* Eq. (3)). C_{target} is target tested into *D* and *k* is iteratively altered until C_{target} is optimized to best fit *D* [26]. The objective function used for the optimization algorithm is shown in Eq. (9) [27]. (*e* is the error, *I* the identity matrix, and *U* an orthonormal matrix spanning the row space of *D*; *U* is calculated by SVD of *D*)

$$e = \left\| (I - U \cdot U^T) \cdot C_{target} \right\|^2 \tag{9}$$

Geometrically speaking, $(I - U \cdot U^T)$ is a projection matrix. If C_{target} represents the true concentration profiles, it is correctly projected into the data space *D* and *e* vanishes [28].

Problems in optimization occur due to local minima. We addressed this by applying a second objective function to check if the same minimum is found by the optimization algorithm. This was based on a Nonlinear Least-Squares approach [29] with the objective function depicted in Eq. (11). Equation (10) merely corresponds to the aforementioned data reduction by factor analysis (*V* is an orthonormal matrix spanning the column space of *D* and calculated by SVD of *D*). Since *V* represents the factor space, the dimension of D_V is smaller than that of *D* without significant loss of informa-

tion. This considerably reduces computational memory requirements.

$$D_V = D \cdot V \tag{10}$$

$$e = \|(I - C_{target} \cdot C^{+}_{target}) \cdot D_V\|^2 \tag{11}$$

Using Eq. (11), k is modified to keep the iterative process going until D is best reproduced similar to Eq. (6). Furthermore, instead of using only the *Frobenius* norm as depicted in Eqs. (9) and (11) we additionally used objective functions based on *DW* [25]. When Eqs. (9) and (11) are not squared elementwise and summed, e is not a scalar but a matrix E. The elements of E are compared using *DW* giving a scalar value (in analogy to e) which accounts for the randomness in E. If E represents a true error, its values will be uncorrelated and random. Thus, a high value using *DW* indicates the best fit. We used the negative of this values (with the best fit being the smallest number) which resulted in another optimization to a minimum.

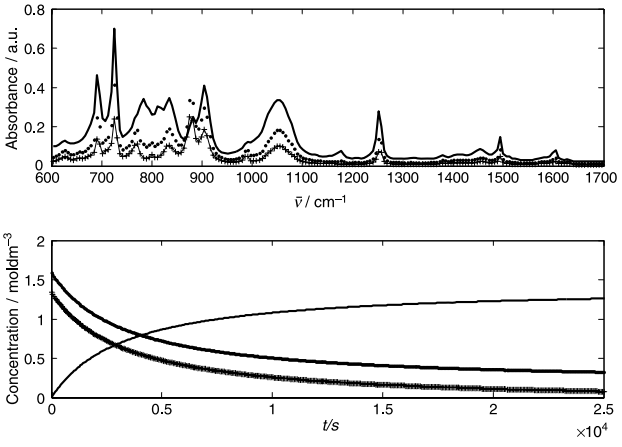

Fig. 4. Spectra (above) and concentration profiles (below) as calculated by SMCR. In both figures '•' denotes **1**, '··+··' denotes **2**, and '—' denotes **4**

All four optimizations converged (with the change in e being less than $\varepsilon = 10^{-100}$) and gave $k = 2.03 \times 10^{-4}\,\mathrm{dm^3\,mol^{-1}\,s^{-1}}$ (at 60°C with 120 ppm Pt). The resulting concentration profiles and spectra are shown in Fig. 4.

These spectra are much smoother than those recovered by ALS. Like in Fig. 2 the spectra of the two educts are calculated to be similar. The calculated educt spectrum is a mixture of the pure component spectra of both educts and the solvent which is attributed to the aforementioned linear dependencies in chemical reactions when components react in parallel. The educt and product spectra highly overlap which is why a second order reaction kinetic was not evident from D and its peak profiles.

Finally, the reaction power was monitored parallel with conversion. Integration of the power gives a reaction enthalpy of 110 kJ/mol (at 60°C, based on divinylbenzene); a maximal power of 220 W/kg (based on the total reaction mass) is released within the first minute.

Polymer Backbone and Polymer Properties

The newly formed Si–C bond may be α or β relative to the phenyl-ring.

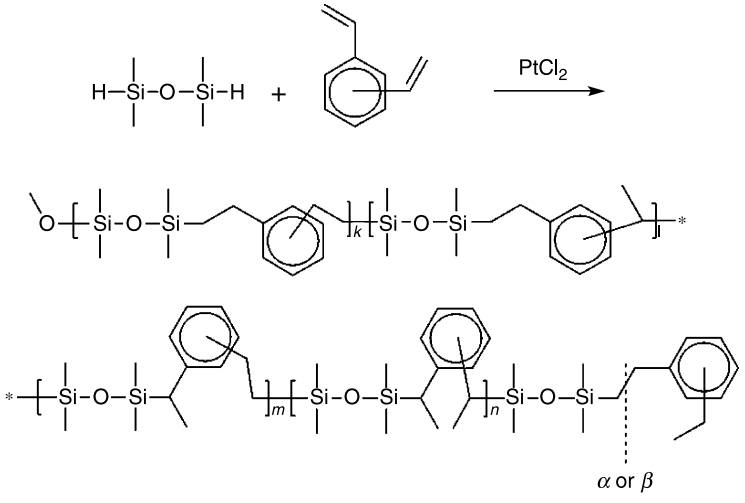

Scheme 2

The presence of the two reaction pathways and the structure of the polymeric backbone was unambiguously resolved by H,H-COSY and ^{1}H NMR experiments. The ratio of β- to α-reaction is 7:3 in accordance with Ref. [14]. Compound **4** was precipitated by addition of methanol which gave rise to hydrogen evolution due to reaction of the excess siliconhydrides with methanol. This process was confirmed by NMR. First, an NMR-sample taken directly from the reaction mixture showed siliconhydrides while an NMR from the purified product lacked those signals, yet showed a multiplet at 3.3 ppm (all in benzene-d_6). Second, this multiplet at 3.3 ppm was assigned by HSQC-DEPT to be a silicon-methoxy group.

Size Exclusion Chromatography (SEC) shows oligomeric fractions in the product and a detached elution peak with $M_n = 88800\,\mathrm{g/mol}$ (polydispersity index (PDI) 3.5). If the oligomeric fractions are integrated into analysis, $M_n = 2900\,\mathrm{g/mol}$ (PDI 62). The *Carothers*-Equation [16] allows calculating the degree of polymerization (X_n) from conversion p and non-stoichiometry r.

$$X_n = \frac{1 + r}{1 + r - 2 \cdot r \cdot p} \tag{12}$$

Taking the calculated $X_n = 11.6$, the molecular weight of the polymer can be estimated to $M_n = 3060\,\mathrm{g/mol}$. Since the reaction was allowed to proceed to full conversion, the high polydispersity of **4** is due to stoichometric mismatch, which in turn results from the ethylvinylbenzene present in **2** (*cf.* Experimental).

Experimental

Siloxane **1** is an in-house product of Wacker Chemie AG. Compounds **2**, **3**, toluene, methanol, and benzene-d_6 were purchased from VWR. While **3**, methanol, and benzene-d_6 were used without further purification, **1**, **2**, and toluene were freshly distilled under N_2. Divinylbenzene **2** was of technical grade; that is, besides consisting of *o*- and *p*-isomers, the corresponding ethylvinylbenzene isomers were present. After distillation under N_2 the amount of ethylvinylbenzene was 35 mol% by NMR.

Experiments were performed in a heat-flow reaction calorimeter (CPA202, ChemiSens) and monitored using an ATR immersion probe (Infrared Fiber Sensors) coupled *via* silver halide fiber optics to a FTIR-spectrometer (Nicolet 380, Thermo Electron Corporation). In a typical run 40 cm^3 toluene, 23 cm^3 **1**, and 18 cm^3 **2** were heated to 60°C. Reaction was initiated by addition of 8.4 mg **3** (dissolved in 1 cm^3 **2**). Thus, the reaction content was 40 cm^3 solvent, 120 ppm Pt, 0.130 mol **1**, and 0.133 mol **2**; the latter needs to be corrected due to the presence of ethyl groups (*vide supra*) to 0.110 mol. The reaction was vigorously stirred and kept isothermal at 60°C until total consumption of **2**. The non-isothermal experiment was started in isothermal mode at 40°C for 50 min, then raised to 70°C with a heating rate of 0.5 K/min, and kept in isothermal mode at 70°C until total consumption of **2**. IR spectra were recorded every minute. The product was precipitated by addition of methanol, decanted, and dried. No attempt was made to extract the remaining catalyst. Thus, the initially yellow precipitate turns black during isolation. The polymer **4** was analyzed by Differential Scanning Calorimetry (DSC) and showed a glass transition temperature $T_g = -77.5$°C ($dT/dt = 10\,\mathrm{K/min}$, Mettler Toledo DSC 821). Molecular weight was determined by SEC (*cf.* Polymer Backbone and Polymer Properties) at 45°C (PLgel 5 μm MIXED-C Column, Polymer Laboratories) against polystyrene standards using toluene as the mobile phase and a refractive index detector (Shodex RI-101). NMR spectra were measured in benzene-d_6 (Bruker AVANCE 400 and Bruker AVANCE 500) at 25°C and are listed in ppm referenced using the solvent peak. The density of the reaction mixture was measured (PAAR Physica DMA 55) and does not deviate from ideality. Thus, volumetric concentrations were used throughout.

Poly[1,1,3,3-tetramethyl-1-(vinylphenyl)ethyl-disiloxane] (**4**, $C_2H_5(C_{14}H_{24}OSi_2)_nOCH_3$)
Prepared according to the description above; ^{1}H NMR (400 MHz, benzene-d_6): $\delta = 7.25$–6.90 (m, aromatic H), 3.30 (m, OCH_3), 2.75 (m, CH_2), 2.20 (m, CH), 1.45 (m, CH_3), 1.00 (m, CH_2), 0.20 (m, $SiCH_3$) ppm; ^{13}C NMR (125 MHz, benzene-d_6): $\delta = 128.4$ (aromatic CH), 125.4 (aromatic CH), 50.6 (OCH_3), 31.9 (CH), 30.0 (CH_2), 21.3 (CH_2), 15.0 (CH_3), 0.6 ($SiCH_3$) ppm; IR (Diamond-ATR): $\bar{\nu} = 3080$, 3020, 2960, 2920, 2860, 1610, 1490, 1450, 1400, 1380, 1250, 1180, 1050, 900, 830, 810, 780, 730 cm^{-1}.

All calculations were performed in Matlab version 7.1 (Mathworks). Though the differential equations of the present system are analytically solvable, all equations were solved numerically using the already implemented algorithms for ordinary differential equations (ode15s). The optimization algorithm was gradient based (lsqnonlin, Optimization Toolbox). Instead of calculating the pseudoinverse, Eqs. (4) and (5) were solved using the Fast Non Negative Least Squares algorithm (FNNLS) [30]. This as well as the ALS algorithm are part of the PLS_Toolbox (Eigenvector Research).

Acknowledgements

We are grateful to Dr. *S. Altmann* and *A. Demmelmair* from the NMR laboratory at Wacker Chemie AG for fruitful discussion and measurement of the NMR spectra. The SEC and density measurements of the analytical laboratories at Wacker Chemie AG and the DSC measurements of the R&D polymers laboratory at Wacker Polymer Systems are gratefully acknowledged.

References

[1] For reviews and selected publications, also including other transition metal catalysts than platinum, see: a) Imlinger NC, Wurst K, Buchmeiser MR (2005) J Organomet Chem **690**: 4433; b) Imlinger NC, Wurst K, Buchmeiser MR (2005) Monatsh Chem **136**: 47; c) Bantu B, Wang D, Wurst K, Buchmeiser MR (2005) Tetrahedron **61**: 12145; d) Glaser PB, Tilley TD (2003) J Am Chem Soc **125**: 13640; e) Marciniec B (2002) Silicon Chemistry **1**: 155; f) Dioumaev VK, Bullock RM (2000) Nature **424**: 530; g) Fu P-F, Brard L, Li Y, Marks TJ (1995) J Am Chem Soc **117**: 7157; h) Brookhart M, Grant BE (1993) J Am Chem Soc **115**: 2151; i) Uozumi Y, Kitayama K, Hayashi T (1993) Tetrahedron: Asymmetry **4**: 2419

[2] Speier JL, Webster JA, Barnes GH (1957) J Am Chem Soc **79**: 974

[3] Brook MA (2000) Silicon in Organic, Organometallic, and Polymer Chemistry, John Wiley & Sons, New York

[4] a) Louis E, Jussofie I, Kühn FE, Herrmann WA (2006) J Organomet Chem **691**: 2031; b) Mukbaniani O, Tatrishvili T, Titvinidze G, Mukbaniani N (2006) J Appl Polym Sci **101**: 388; c) He X, Herz J, Guenet J-M (1987) Macromolecules **20**: 2003

[5] a) Sia SK, Whitesides GM (2003) Electrophoresis **24**: 3563; b) Campbell DJ, Beckman KJ, Calderon CE, Doolan PW, Ottosen RM, Ellis AB, Lisensky GC (1999) J Chem Educ **75**: 537

[6] a) Sargent JR, Weber WP (1999) Macromolecules **32**: 2826; b) Hu J, Son DY (1998) Macromolecules **31**: 4645; c) Dvornic PR, Gerov VV, Govedarica MN (1994) Macromolecules **27**: 7575

[7] Blackmond DG (2005) Angew Chem **117**: 4374

[8] Brendel M, Bonvin D, Marquardt W (2006) Chem Eng Sci **61**: 5404

[9] a) Puxty G, Maeder M, Hungerbühler K (2006) Chemom Intell Lab Syst **81**: 149; b) Carvalho AR, Wattoom J, Zhu L, Brereton RG (2006) Analyst **131**: 90; c) Allian AD, Tjahjono M, Garland M (2006) Organometallics **25**: 2182; d) Diewok J, de Juan A, Maeder M, Tauler R, Lendl B (2003) Anal Chem **75**: 641; e) Tauler R, Smilde AK, Henshaw JM, Burgess LW, Kowalski BR (1994) Anal Chem **66**: 3337; f) Henshaw JM, Burgess LW, Booksh KS, Kowalski BR (1994) Anal Chem **66**: 3328

[10] a) Jiang J-H, Liang Y, Ozaki Y (2004) Chemom Intell Lab Syst **71**: 1; b) Windig W (1988) Chemom Intell Lab Syst **4**: 201; c) Lawton WH, Sylvestre EA (1971) Technometrics **13**: 617

[11] Malinowski ER (2002) Factor Analysis in Chemistry, John Wiley and Sons, New York

[12] Frans SD, Harris JM (1985) Anal Chem **57**: 1718

[13] Gemperline PJ (1999) Anal Chem **71**: 5398

[14] Caseri W, Pregosin PS (1988) J Organomet Chem **356**: 259

[15] Lin-Vien D, Colthup NB, Fateley WG, Grasselli JG (1991) The Handbook of Infrared and Raman Characteristic Frequencies of Organic Molecules, Academic, San Diego

[16] Tieke B (2005) Makromolekulare Chemie: Eine Einführung, WILEY-VCH, Weinheim

[17] Shrager RI (1986) Chemom Intell Lab Syst **1**: 59

[18] Henrion R, Henrion G (1994) Multivariate Datenanalyse: Methodik und Anwendung in der Chemie und verwandten Gebieten, Springer, Berlin

[19] Ruckebusch C, de Juan A, Duponchel L, Huvenne JP (2006) Chemom Intell Lab Syst **80**: 209

[20] Amrhein M, Srinivasan B, Bonvin D, Schumacher MM (1996) Chemom Intell Lab Syst **33**: 17

[21] a) Domínguez-Vidal A, Saenz-Navajas MP, Ayora-Canada MJ, Lendl B (2006) Anal Chem **78**: 3257; b) de Juan A, Maeder M, Martinez M, Tauler R (2000) Chemom Intell Lab Syst **54**: 123; c) Tauler R, Smilde A, Kowalski B (1995) J Chemom **9**: 31

[22] Malinowski ER (1977) Anal Chem **49**: 606

[23] Meloun M, Capek J, Miksik P, Brereton RG (2000) Anal Chim Acta **423**: 51

[24] Chen Z-P, Liang Y-Z, Jiang J-H, Li Y, Qian J-Y, Yu R-Q (1999) J Chemom **13**: 15

[25] a) Windig W (2005) Chemom Intell Lab Syst **77**: 206; b) Gourvénec S, Massart DL, Rutledge DN (2002) Chemom Intell Lab Syst **61**: 51

[26] a) Puxty G, Maeder M, Rhinehart RR, Alam S, Moore S, Gemperline PJ (2005) J Chemom **19**: 329; b) Furusjö E, Danielsson L-G (1998) Anal Chim Acta **373**: 83; c) Knorr FJ, Harris JM (1981) Anal Chem **53**: 272

[27] a) Furusjö E, Danielsson L-G (2000) J Chemom **14**: 483; b) Furusjö E, Danielsson L-G (2000) Chemom Intell Lab Syst **50**: 63

[28] Lorber A (1984) Anal Chem **56**: 1004

[29] Maeder M, Zuberbühler AD (1990) Anal Chem **62**: 2220

[30] Bro R, de Jong S (1997) J Chemom **11**: 393